

Accepted Manuscript

Design, synthesis and biological evaluation of novel oseltamivir derivatives as potent neuraminidase inhibitors

Zhen Wang, Li Ping Cheng, Xing Hua Zhang, Wan Pang, Liang Li, Jin Long Zhao

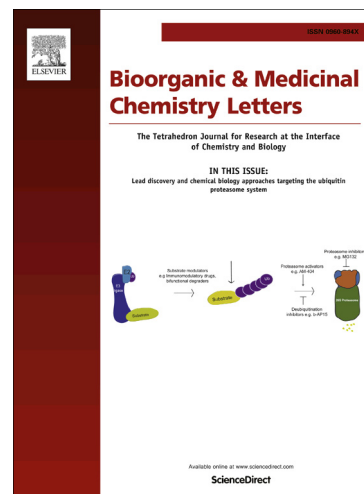
PII: S0960-894X(17)31079-X
DOI: <https://doi.org/10.1016/j.bmcl.2017.11.003>
Reference: BMCL 25409

To appear in: *Bioorganic & Medicinal Chemistry Letters*

Received Date: 6 August 2017
Revised Date: 27 October 2017
Accepted Date: 2 November 2017

Please cite this article as: Wang, Z., Cheng, L.P., Zhang, X.H., Pang, W., Li, L., Zhao, J.L., Design, synthesis and biological evaluation of novel oseltamivir derivatives as potent neuraminidase inhibitors, *Bioorganic & Medicinal Chemistry Letters* (2017), doi: <https://doi.org/10.1016/j.bmcl.2017.11.003>

This is a PDF file of an unedited manuscript that has been accepted for publication. As a service to our customers we are providing this early version of the manuscript. The manuscript will undergo copyediting, typesetting, and review of the resulting proof before it is published in its final form. Please note that during the production process errors may be discovered which could affect the content, and all legal disclaimers that apply to the journal pertain.





Design, synthesis and biological evaluation of novel oseltamivir derivatives as potent neuraminidase inhibitors

Zhen Wang, Li Ping Cheng^{a,*}, Xing Hua Zhang, Wan Pang, Liang Li, Jin Long Zhao

^aSchool of Chemical and Environmental Engineering, Shanghai Institute of Technology, Shanghai 201418, China

ARTICLE INFO

Article history:

Received 6 August 2017

Revised 26 September 2017

Accepted

Available online

Keywords:

Neuraminidase inhibitors

3D-QSAR

Molecular docking

Molecular dynamics simulations

Oseltamivir derivatives

ABSTRACT

Neuraminidase (NA) is one of the particular potential targets for novel antiviral therapy. In this work, A series of neuraminidase inhibitors with the cyclohexene scaffold were studied based upon the combination of 3D-QSAR, molecular docking, and molecular dynamics techniques. The results indicate that the built 3D-QSAR models yield reliable statistical information: the correlation coefficient (r^2) and cross-validation coefficient (q^2) of CoMFA (comparative molecular field analysis) are 0.992 and 0.819; the r^2 and q^2 of CoMSIA (comparative molecular similarity analysis) are 0.992 and 0.863, respectively. Molecular docking and MD simulations were conducted to confirm the detailed binding mode of enzyme-inhibitor system. The new NA inhibitors had been designed, synthesized, and their inhibitory activities against group-1 neuraminidase were determined. One agent displayed excellent neuraminidase inhibition, with IC_{50} value of 39.6 μ M against NA, while IC_{50} value for oseltamivir is 61.1 μ M. This compound may be further investigated for the treatment of infection by the new type influenza virus.

2009 Elsevier Ltd. All rights reserved

As worldwide epidemic strains, influenza can cause acute respiratory diseases and annual influenza pandemic. The swine-origin H1N1 influenza virus unleashed a severe public panic in 2009.¹ It is reported that highly pathogenic influenza virus H5N1 can lead to an alarming life threatening (60% mortality),^{2,3} and recent studies have raised a major concern on possible transmission of avian influenza virus H5N1 to humans. A lethal avian influenza H7N9 has evolved to influence human since 2013, endemic to China.

Neuraminidase (NA), a membrane-bound glycoprotein, playing a dominant role in the viral life cycle.⁴ The phylogenetic tree divides all neuraminidase subtypes into two groups,⁵ there exists a large cavity (termed 150-cavity) in group-1 NAs, adjacent to the active site of proteins, whereas that is not found in group-2 NAs.⁶ Neuraminidase inhibitors (NAIs) had been regarded as the most potent agents to cure influenza disease. Up to now, four NA inhibitors have been developed as efficacious treatment of influenza infections: oseltamivir (1), zanamivir (2), peramivir (3), and laninamivir (4) (Figure 1).⁷ Among these, orally administered oseltamivir (OS) has been posed to treat broader cases since its approval in 1999, while recently, several reported oseltamivir-resistant strains have seriously limited the drug's clinical application.⁸⁻¹² Zanamivir is primarily administered by inhalation via a nebulizer or intravenous channels.¹³ Peramivir has been authorized in the Republic of Korea and China, and laninamivir have to date been approved as

antiviral drugs in Japan.¹⁴⁻¹⁵ Nevertheless, variant strains that are against these drugs are also continuously been discovered.

Recent papers have reported some progresses in NA and its inhibitors in theoretical and experimental studies. For instance, Chen et al.¹⁶ discovered a series of crenatoside analogues as novel influenza neuraminidase inhibitors, identified by biological evaluation. Hoffmann et al.¹⁷ developed a platform for determining the inhibition profile of NAIs in the N1 background. In addition, Xie et al.¹⁸ had designed and synthesized two series of oseltamivir derivatives. Of these, two compounds obtained by introduction of biphenyl substituents into the C-5 NH_2 position exhibited comparable or even better inhibitory activities relative to the OS carboxylate against N1.

In this work, 65 oseltamivir analogs were selected as dataset.^{18,19} Some studies were employed using computational methods including 3D-QSAR, molecular docking and MD simulations. The results of CoMFA and CoMSIA supply insights into key structural factors required for the neuraminidase inhibition.^{20,21} Molecular docking and MD simulations were performed to validate the 3D-QSAR models and quantify the interactions of NA-ligand.²²⁻²⁷ Previous studies showed that the biphenyl substituents introduced into C5- NH_2 of ligand could improve compound's biological activity.²⁸⁻³⁰ In terms of substituent's structure, the chemical bonds between the biphenyl groups can be freely rotated, this increases the opportunity to interact with neighbouring amino acid residues. Accordingly,

*Corresponding authors. Tel.: +86 21 60873250; fax: +86 21 60 877231 (L.C.).
E-mail address: chengliping@sit.edu.cn (L. Cheng).

some new oseltamivir derivatives were designed by introduction of biphenyl substitutes into the C5 NH₂ position based on the built 3D-QSAR contour maps. Finally, the new designed molecules were further confirmed by experimental synthesis and biological evaluation.

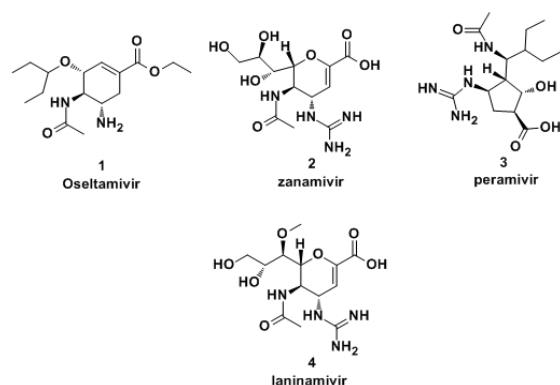


Figure 1. Structures of the approved NA inhibitors 1-4.

The 65 oseltamivir derivatives in this paper randomly divided into 55 training set compounds (84.6%) for model generation and 10 test set compounds (15.4%) for model validation. The chemical structures, active values against neuraminidase subtype 1 are listed in Supplementary Information (Table S1). To build more reliable and statistical 3D-QSAR models, we corrected the active data originating in two independent documents to eliminate errors. The specific method is as follows: the IC₅₀ active values were converted into the corresponding pIC₅₀ (-logIC₅₀) values, then the pIC₅₀ values were transformed into superior pIC_{50c} values (pIC_{50c}), used as dependent variables to build molecular models. pIC_{50c} values were obtained according to the following formula³¹:

$$pIC_{50c} = pIC_{50} / pIC_{50}(\text{OS-C}) \quad (1)$$

Where pIC₅₀, pIC₅₀(OS-C) represent the experimental bioactive data of the data set compounds and oseltamivir carboxylate (OS-C), respectively.

Table 1. Statistical results and relative contributions of the models

Methods ^a	CoMFA	CoMSIA
q^2	0.819	0.863
Noc	8	9
r^2	0.992	0.992
SEE	0.013	0.014
F-test	700.919	607.026
Relative contributions		
Steric	0.450	0.129
Electrostatic	0.550	0.280
H-donor	—	0.199
H-acceptor	—	0.106
Hydrophobic	—	0.286

independent variable.

In this study, the ligand-based alignment rule was used. The alignment result is shown in Figure 2. We performed regression analysis using partial least squares (PLS) to evaluate and judge merits or demerits of the model with some statistical parameters, including r^2 , q^2 , standard error of estimate (SEE) and F-test values. The best optimal value of CoMFA and CoMSIA models are listed in Table 1. From this, we observed both models show satisfactory predictive capability, with q^2 , r^2 , and SEE are 0.819, 0.992, 0.013 for CoMFA model, and 0.863, 0.992, 0.014 for CoMSIA model. In Figure 3, the linear fit between actual and

predicted activity of the best optimal CoMFA and CoMSIA model is described, the residual values of drugs between the predicted and actual pIC₅₀ exceeded 1 logarithm unit is treated as outliers (compounds **56** and **60**).³² Actually, when the classical internal validation parameter q^2 is greater than 0.5, a model is reassuring and predictive.^{33,34} Determined by leave-one-out validation, the optimal principal components of CoMFA and CoMSIA are 8 and 9, respectively. The F-test values are 700.919 and 607.026 for CoMFA and CoMSIA, respectively, a model is statistically significant with high F-test value. The allocation proportion of steric and electrostatic fields is 0.450 and 0.550, respectively. For the chosen CoMSIA model, the relative contribution of steric, electrostatic, hydrophobic, H-bond donor and acceptor fields are 0.129, 0.277, 0.286, 0.199 and 0.106, respectively. The paramount contribution in the model is hydrophobic interaction.

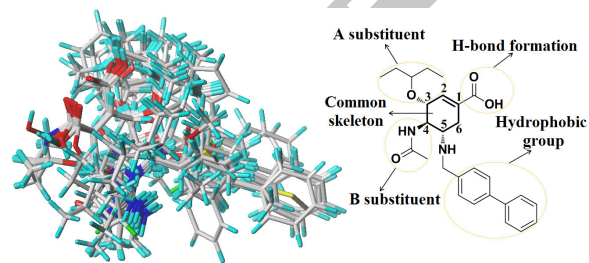


Figure 2. Superimposition of the training set and compound **25** used as a template for alignment. Molecules are colored in white for common C, cyan for H, red for O, blue for N, yellow for S, green for F, Cl & Br, respectively. The common substructure is cyclohexene (shown in bold), and other important substituents involving A, B, H-bond formation substituent and hydrophobic groups, shown in dashed orange frame.

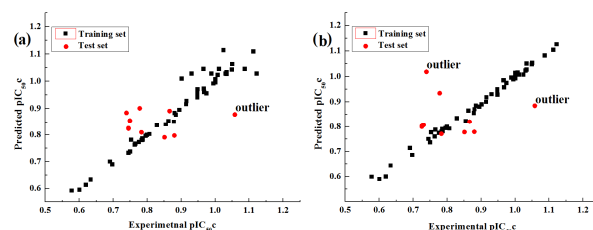


Figure 3. Scatter plot of experimental pIC_{50c} versus activity predicted by the optimal CoMFA (a) and CoMSIA (b) model.

For convenient analysis, N-substituted neuraminidase inhibitors were separated into four regions: H-bond formation in C1 position; C3- ethylprooxy; C4-acylamino; hydrophobic group in C5 position. The 3D contour maps of CoMFA and CoMSIA models are explained in Figure 4~6. From these, we can interpret the key structural features required for inhibitory activity.

Figure 4a and 4b represent the steric contour maps of CoMFA and CoMSIA, respectively. Steric favored in green and the yellow body indicated negative spatial factor. The default value of field favored and disfavored proportion are 80% and 20% level contribution. It could be observed that the inhibitory activity of compound **09** is lower than that of compound **07** from Supplementary Information (Table S1), because more potent compound **07** has larger functional groups at the C5 region, the same case with compounds **08** and **10**. A large green contour may be favorable to cover the benzene groups, for example, molecules **25**, **26**, **29** and **31** show excellent inhibitory activities with such substituents at this position. However, the C5-NH₂ position with too large group would have adverse effect on

bioactivity, such as compounds **25** and **30**, which indicates that the appropriate bulky groups are beneficial to inhibitory activity. In addition, if the C3 position is replaced with $-NH_2$ group, molecules would possess weaker inhibitory ability even there exists bulky groups, such as compounds **49** and **53-55**. From Figure 4b, it could be inspected that the CoMSIA contour maps hold similar modes with that of CoMFA.

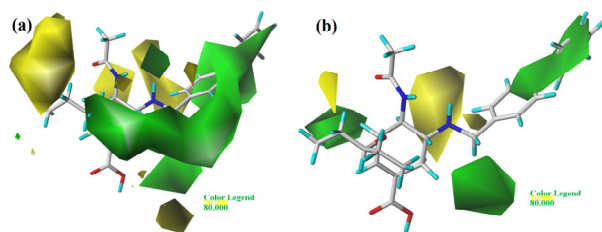


Figure 4. Steric contour maps of CoMFA (a) and CoMSIA (b). The green color shows the favored steric area and the yellow color shows disfavored steric area.

From Figure 5, the red (electronegative groups favored) and blue (electropositive favored) contours also represent default level contributions. Figure 5a shows that there are three small-sized red contours near the $-COO^-$, a medium-sized red contour around the C3-methoxypentane, suggesting that the electronegative groups are favored to bioactivity. One piece of medium-sized red contour at the biphenyl group indicates the importance of electronegative substituents in imparting better biological activity. Therefore, compound **30** acts decreased inhibitory activity compared to compound **29**, and it is thus feasible to introduce advisable electronegative groups to the C5- NH_2 substituent to obtain high active molecules. One could observe that the compounds with too strong electronegative groups would lead to a decreased biological activity. For example, the inhibitory capacity of compound **23** is inferior to that of compound **22**, because the strong electronegativity of F atom slightly inactivates the biphenyl-correlated drugs. Figure 5b represents the CoMSIA electrostatic contour maps. Compared with the CoMFA contour maps, there is only one small-sized red contour around $-COO^-$. A medium-sized blue contour surrounds $-NHAc$, showing that the electropositive substituents are beneficial to compounds inhibitory activity.

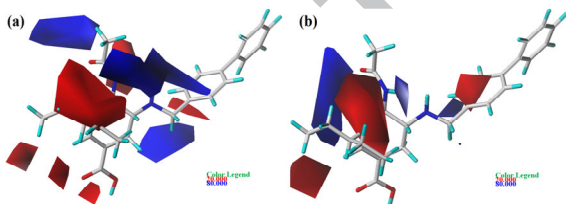


Figure 5. Electrostatic contour maps of CoMFA (a) and CoMSIA (b). Electrostatic fields: favored (red) and disfavored (blue).

As shown in Figure 6, the yellow pieces denote that hydrophobic groups are beneficial to inhibitors biological activity and the white regions reveal that the hydrophilic substituents may be tolerated. The C5- NH_2 group of oseltamivir is close to NA active pocket. One large yellow contour surrounding C5- NH_2 suggests that the existence of hydrophobic R^1 group is advantageous to bioactivity. For example, the high bioactivity of **25** appears to be partly dependent upon the hydrophobic biphenyl group at this site. The change of hydrophobic and hydrophilic circumstance around C3-ethylpropoxy greatly influenced compounds inhibitory activity, maintaining the original structure of C3-substituents is reasonable.

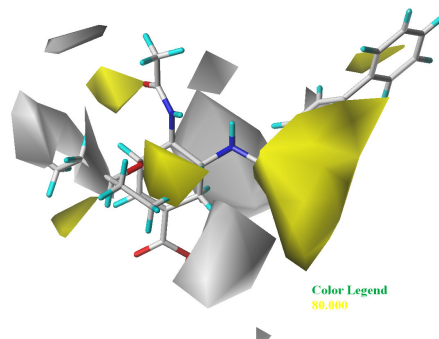


Figure 6. Hydrophobic contours of CoMSIA model. The yellow shows the favored hydrophobic area and the white color shows the disfavored hydrophobic area.

Docking results show that the highest total-score of compound **25** is 11.35, the total-score of docking studies are shown in Table S2 (Supplementary Information). Based on the contour maps obtained from 3D-QSAR models and the structural features of the most active molecule **25**, some new compounds **3-7** were designed by introduction of various substituents into the biphenyl moiety at the C5- NH_2 position. The docking scores and the predicted pIC_{50} and pIC_{50c} values of **3-7** based on CoMFA and CoMSIA models are listed in Table S3 (Supplementary Information). Table S3 shows that the predicted and docking values of all designed molecules are equally high with those of oseltamivir, suggesting their good inhibitory activity and potent binding affinity with receptor. Among these new compounds, **3** has the highest docking score (**11.37**) and inhibitory activity predicted by both CoMFA and CoMSIA models, it was subsequently synthesized and evaluated for NA inhibition. Compound **4** was designed based on the molecular structure of oseltamivir, it does not possess the highest predictive value.

To better understand the discrepancy of activity between compounds oseltamivir, **3** and **4** we compared their 3D binding modes with NA derived from docking simulation. As shown in Figure 7a, although oseltamivir (in purple) could occupy the active site of NA, it is powerless to bond well with the 150-cavity. Compound **3** (in green) had the ability to perfectly dock into the interaction site of NA, and the biphenyl moiety of **3** appropriately embedded within the 150-cavity, which is the crucial binding site of group-1 NA. Nevertheless, compound **4** (in cyan) was out of the active site and the corresponding biphenyl moiety could not occupy the 150-cavity. In addition, from previous study, we found that binding interaction of the biphenyl group with enzyme was hydrophobic. Figure 7b clearly shows that most amino acids near this group are hydrophobic, such as Trp178, Val149, and Arg224. The side chains of Arg292, Arg371, and Glu276 also contribute significantly to the hydrophobicity of the 150-cavity.

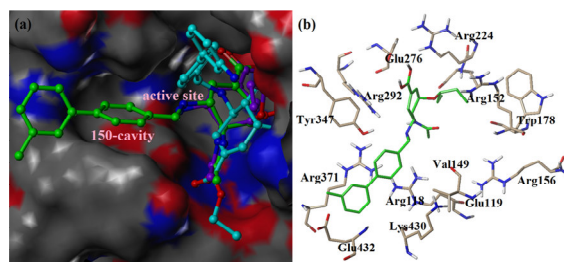


Figure 7. The binding models of compounds oseltamivir (purple), **3** (green) and **4** (cyan) with N1 (PDB 2HU0), (a) and the key residues that may form potential interactions with compound **3** (b).

The difference in inhibitory activity for **1**, **3** and **4**, may be also interpreted by the number of hydrogen bonds formed by inhibitor and enzyme. Figure 8a illustrates hydrogen bonding interactions between compound oseltamivir and key residues (Arg152, Arg292, and Arg371) in the active site. A total of four hydrogen bonds were formed. Figure 8b illustrates hydrogen bonding interactions between compound **3** and key residues (Arg152, Arg292, Arg371, and Tyr347) in the active site. A total of six hydrogen bonds were formed. The hydrogen bond distances captured are 1.75 Å (Arg152-HN-H...O-CCH₃-NH), 2.01 Å (Arg292-HN-H1...OHCO), 2.24 Å (Arg292-HN-H2...OHCO), 1.91 Å (Arg371-HN-H1...OHCO), 2.54 Å (Arg371-HN-H...O-COH), and 2.50 Å (Tyr347-HC-H...OHCO), respectively. Figure 8c illustrates hydrogen bonding interactions between compound **4** and key residues (Arg152, Tyr347) in the active site, only two hydrogen bonds were formed. Figure 8d, 8e, 8f show that compounds **5**, **6**, **7** can bind with the receptor for **3**, **4**, **4** hydrogen-bonding, respectively. Thus, it is clearly that the number of hydrogen bonds is correlated to NAIs activity.

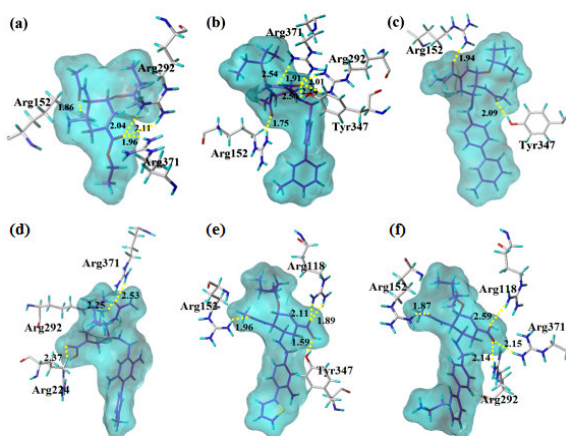


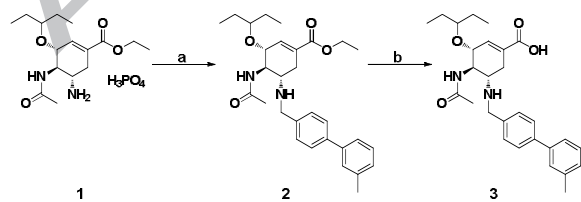
Figure 8. Docking results of the compounds **1** (a), **3** (b), **4** (c), **5** (d), **6** (e) and **7** (f) in the study. The binding site surrounds the ligand. Hydrogen bonds are indicated as yellow dashed lines, with unit distance of Å. Molecular surface is shown as cyan.

Table 2. IC₅₀ ± SD (μM) value of compounds **3** and **1** against NA

	3	1 (oseltamivir)
IC ₅₀ (μM)	39.6 ± 6.5	61.1 ± 6.3

Table 3. IC₅₀ ± SD (μM) value of compounds **3** and **1** against A/WSN/33 H1N1

	3	1 (oseltamivir)
IC ₅₀ (μM)	1.72 ± 0.35	0.579 ± 0.082
CC ₅₀ (μM)	373 ± 19.50	>500



Scheme 1. Synthesis of compounds **3**. Regents and conditions: (a) Aldehyde, EtOH, 30 °C; NaBH₃CN, 30 °C; (b) MeOH, H₂O, NaOH, 55 °C, then acetic acid.

We conducted experimental synthesis to study the predictive compound **3** severely. The major structures and synthetic route

are shown in Scheme 1. The neuraminidase inhibitory assay and virus inhibition results are listed in Table 2 and Table 3, respectively. Experimentally, as shown in Table 2, compound **3** exerts good potency, with IC₅₀ value of 39.6 μM against NA, which is lower than that of oseltamivir (IC₅₀ = 61.1 μM). From Table 3, it can be observed that the inhibitory activity for **3** (IC₅₀ = 1.72 μM) is almost equal to the oseltamivir (IC₅₀ = 0.579 μM), the cytotoxicity for the compound **3** is 373 μM, while the toxicity value for oseltamivir is > 500 μM. Thus, the selective index (SI = CC₅₀/IC₅₀) for compound **3** is impressive, indicating that the biphenyl group probably formed some special interactions with the N1 enzyme. The inhibition curve and toxicity test curve of compound **3** against H1N1 virus is shown in Figure S1 (Supplementary Information).

Molecular dynamics (20 ns) for six inhibitors were undertaken to confirm the reliability of docking results. The system stability and overall convergence of simulations were monitored in terms of root-mean-square deviation (RMSD) of NA-inhibitor backbone atoms (C, Cα, N, and O). The average RMSD value of each step versus time of three representative inhibitors is shown in Fig. S2 (Supplementary Information). It can be seen that all complexes except NA- compound **4** are stable after 4 ns, and fluctuations in the average RMSD values during the whole simulation are between 2.0 Å and 4.0 Å, indicating the other complexes keep an approximate invariable state. Figure 9 depicts a superposition of two structures for NA-compound **3**, and there seems to be no significant difference between initial structure (in green) and the lowest energy structure (in pink) except for a slight drift and rotation. The MD simulation results are in good agreement with molecular docking results.

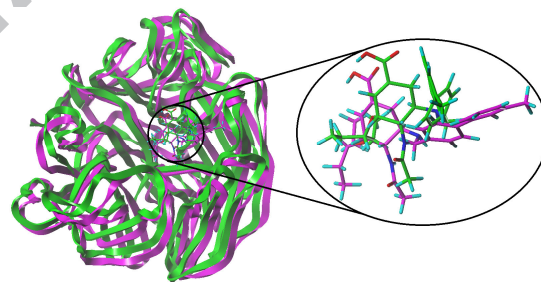


Figure 9. View of superimposed backbone atoms of the initial structure (green) of the MD simulations and the lowest energy structure (pink) for compound **3**-2HU0 complex. Compound **3** represented as carbon-chain in green for the initial complex and carbon-chain in pink for the lowest energy complex.

To quantify the docking results, the binding free energy calculations for the six complexes of the last 2 ns trajectory were performed and are listed in Table S4 (Supplementary Information). MM/GBSA (Molecular Mechanics/Generalized Born Surface Area) and MM/PBSA (Molecular Mechanics/Poisson Boltzmann Surface Area) were applied in free energy calculations. As listed in Table S4, the binding free energies of **1**, **3**-**7** via MM/GBSA were predicted to be -16.27, -23.21, -12.14, -18.85, -14.95 and -12.25 kcal/mol, respectively, and via MM/PBSA were predicted to be -15.29, -22.36, -13.35, -17.23, -14.31 and -13.92 kcal/mol, respectively. It can be detected that all binding free energies of **3**-**7** are more negative than the observed free energy of -10.60 ~ -10.36 kcal/mol for oseltamivir,³⁵ implying that the introduced chemical structures increase the binding affinities of ligands coupling with subtype N1. Among the six compounds, **3** should possess the highest activity on account of its most negative binding free energy. The calculated binding free energies are in good agreement with the 3D-QSAR predicted results.

In this paper, a series of N-substituted oseltamivir derivatives were studied by computer-aided drug design processes, such as 3D-QSAR, molecular docking and molecular dynamics simulations. The built 3D-QSAR models exhibit excellent internal predictive activity, which can be extrapolated to design new and more robust inhibitors. Docking results show that the main residues in the active pocket 2HU0 are hydrophobic, and Arg152, Arg292, Arg371 are key residues. Hydrogen bond and hydrophobic interactions play key roles in binding of inhibitors and NA. MD simulations were carried out for designed potential compounds to verify the docking results. A novel oseltamivir derivative was further synthesized in good yield with an optimized strategy. The compound were then screened for its bioactivity against neuraminidase and H1N1 virus in liquid media and fluorescence detection. Compound **3** shows even better inhibitory activity relative to the compound **1** (oseltamivir). In conclusion, the N-substituted oseltamivir analogs discussed in this paper provided neoteric viewpoint on enhancing drugs inhibitory activity.

Acknowledgments

Thanks for financial support given by Natural Science Foundation of Shanghai (No. 15ZR1440400), National Youth Fund Project of China (No. 21602135), Collaborative Innovation Fund (XTCX2016-14), Shanghai Municipal Education Commission (Plateau Discipline Construction Program), and the National Natural Science Foundation of China (No. 21472126). Authors are also thankful to Jinan Huawei Pharmaceutical Com. Ltd. and Institut Pasteur of Shanghai for their help in neuraminidase inhibitory assay and virus inhibitory assay.

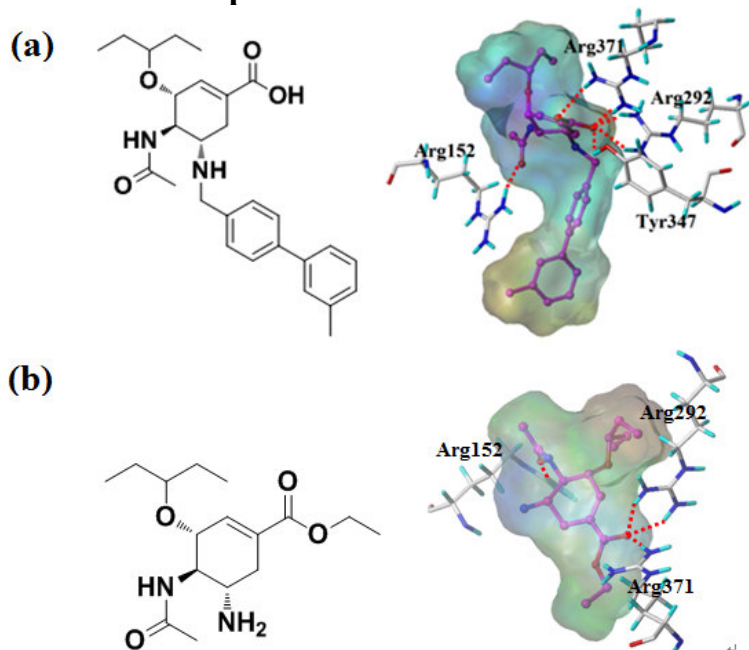
Supplementary data

Materials and Methods, Table S1, Table S2, Table S3, Table S4, Figure S1, Figure S2, 1H NMR and 13C NMR spectra, HRMS spectra for the new drug associated with this paper.

References and notes

- Mooney, C. A.; Johnson, S. A.; P. T. H.; Quarles, v. U. L.; de Haan, C. A.; Moret, E. E.; et al. *J. Med. Chem.* **2014**, *57*, 3154-3160.
- Niikura, M.; Bance, N.; Mohan, S.; Pinto, B. M. *Antivir. Res.* **2011**, *90*, 160-163.
- Greenway K T.; Legresley E B.; Pinto B M. *Plos One.* **2013**, *8*, e59873.
- Schade, D.; Kotthaus, J.; Riebling, L.; Kotthaus, J.; Müller-Fielitz, H.; Raasch, W.; ... Clement, B. *J. Med. Chem.* **2014**, *57*, 759-769.
- Mallipeddi, P. L.; Kumar, G.; White, S. W.; Webb, T. R. *Curr. Top. Med. Chem.* **2014**, *14*, 1875-1889.
- Cheng, L. P.; Huang, X. Y.; Wang, Z.; Kai, Z. P.; Wu, F. H. *Monatsh. Chem.* **2014**, *145*, 9-22.
- Adabala, P. J. P.; LeGresley, E. B.; Bance, N.; Niikura, M.; Pinto, B. M. *J. Org. Chem.* **2013**, *78*, 10867-10877.
- Sun J.; Mei H. *Chemometr. Intell. Lab.* **2015**, *146*, 485-493.
- Wang, Z.; Cheng, L.; Kai, Z.; Wu, F.; Liu, Z.; Cai, M. *Bioorg. Med. Chem. Lett.* **2014**, *24*, 3869-3876.
- Gao, L.; Zu, M.; Wu, S.; Liu, A. L.; Du, G. H. *Bioorg. Med. Chem. Lett.* **2011**, *21*, 5964-5970.
- Mckimbreschkin, J.; Trivedi, T.; Hampson, A.; Hay, A.; Klimov, A.; & Tashiro, M.; et al. *Antimicrob. Agents. Chemother.* **2003**, *47*, 2264-2272.
- Gupta R K.; Nguyen-Van-Tam J S. *New. Engl. J. Med.* **2006**, *354*, 1423-1424.
- Hayden, F. G.; Osterhaus, A. D.; Treanor, J. J.; Fleming, D. M.; Aoki, F. Y.; Nicholson, K. G.; et al. *New. Engl. J. Med.* **1997**, *337*, 874-880.
- Chachra, R.; Rizzo, R. C. *J. Chem. Theory. Comput.* **2008**, *4*, 1526-1540.
- Birnkrant D, Cox E. *New. Engl. J. Med.* **2009**, *361*, 2204-2207.
- Chen, B. L.; Wang, Y. J.; Guo, H.; Zeng, G. Y. *Eur. J. Med. Chem.* **2016**, *109*, 199-205.
- Hoffmann, A.; Schade, D.; Kirchmair, J.; Clement, B.; Sauerbrei, A.; Schmidtke, M. *J. Virol. Methods.* **2016**, *237*, 192-199.
- Xie, Y.; Xu, D.; Huang, B.; Ma, X.; Qi, W.; Shi, F.; ... Xu, W. *J. Med. Chem.* **2014**, *57*, 8445-8458.
- Li Y.; Zhou B.; Wang R. *J. Mol. Graph. Model.* **2009**, *28*, 203-219.
- Romero-Parra J.; Chung H.; Tapia R A, et al. *Eur. J. Pharm. Sci.* **2017**, *101*:1.
- Lu P.; Wei X.; Zhang R. *Eur. J. Med. Chem.* **2010**, *45*, 3413-3419.
- Myint K Z.; Xie X Q. *Int. J. Mol. Sci.* **2010**, *11*, 3846-3866.
- Sun, C.; Zhang, X.; Huang, H.; Zhou, P. *Bioorg. Med. Chem.* **2007**, *14*, 8574-8581.
- Yi, X.; Guo, Z.; Chu, F. M. *Bioorg. Med. Chem.* **2003**, *11*, 1465-1474.
- Shu, M.; Lin, Z.; Zhang, Y.; Wu, Y.; Mei, H.; Jiang, Y. *J. Mol. Model.* **2011**, *17*, 587-592.
- Zhu Y L.; Beroza P.; Artis D R. *J. Chem. Inf. Model.* **2014**, *54*, 462-469.
- Mohan, S.; McAtamney, S.; Haselhorst, T.; von Itzstein, M.; Pinto, B. M. *J. Med. Chem.* **2010**, *53*, 7377-7391.
- Albohy, A.; Mohan, S.; Zheng, R. B.; Pinto, B. M.; Cairo, C. W. *Bioorg. Med. Chem.* **2011**, *19*, 2817-2822.
- Collins, P. J.; Haire, L. F.; Lin, Y. P.; Liu, J.; Russell, R. J.; Walker, P. A.; ... Gamblin, S. J. *Nature.* **2008**, *453*, 1258-1261.
- Jones, B. A.; Lessler, J.; Bianco, S.; Kaufman, J. H. *Plos One.* **2015**, *10*, e0137482.
- Selvaraj, C.; Tripathi, S. K.; Reddy, K. K.; Singh, S. K. *Cur. Trends. Biotechnol. Pharm.* **2011**, *5*, 1104-1109.
- Nguyen, H. T.; Nguyen, T.; Mishin, V. P.; Sleeman, K.; Balish, A.; Jones, J.; ... Nguyen, D. T. *Emerg. Infect. Dis.* **2013**, *19*, 1963-1971.
- Roy P P.; Leonard J T.; Roy K. *Chemometr. Intell. Lab.* **2008**, *90*, 31-42.
- Gagic, Z.; Nikolic, K.; Ivkovic, B.; Filipic, S.; Agbaba, D. *J. Taiwan. Inst. Chem. E.* **2015**, *59*, 33 - 44.
- Park J W, Jo W H. *Eur. J. Med. Chem.* **2010**, *45*, 536-541.
- Fu, L.; Bi, Y.; Wu, Y.; Zhang, S.; Qi, J.; Li, Y.; ... Gao, G. F. *J. Med. Chem.* **2016**, *59*, 6303-6012.
- Russell, R. J.; Haire, L. F.; Stevens, D. J.; Collins, P. J.; Lin, Y. P.; Blackburn, G. M.; ... Skehel, J. J. *Nature.* **2006**, *443*, 45-49.
- Chen, B. L.; Wang, Y. J.; Guo, H.; Zeng, G. Y. *Eur. J. Med. Chem.* **2016**, *109*, 199 - 205.
- Liu, A. L.; Wang, H. D.; Lee, M. Y.; Wang, Y. T.; Du, G. H. *Bioorg. Med. Chem.* **2008**, *16*, 7141-7147.

Graphical abstract



Compound **3** (a), $IC_{50} = 39.6 \mu M$, more effective in inhibiting subtype N1 than compound **1** (b) (with IC_{50} value = $61.1 \mu M$); docking results of the potent molecule **3** and **1** binding amino acid residues with hydrogen bonds.